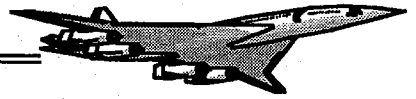

CFD Data Generation Process for Nonlinear Loads

Boeing Long Beach: Alan Arslan, Todd Magee, Eric Unger, Peter Hartwich, Shreekant Agrawal, Joseph Giesing, and Bala Bharadvaj

NASA Ames: Neal Chaderjian and Scott Murman

NASA/Industry HSR Technology Integration Review
Los Angeles, California
February 9-13, 1998

NOTE

This paper was presented in the session entitled "TI Studies related to Configuration Aerodynamics" (CA/TI joint session) on Thursday morning February 12, 1998. The session chairperson was Chet Nelson.

CFD Data Generation Process for Nonlinear Loads

Alan Arslan, Todd Magee, Eric Unger,
Peter Hartwich, Shreekant Agrawal, Joseph Giesing, and Bala Bharadvaj

The Boeing Company
Long Beach, California 90807-5309

Neal Chaderjian, Scott Murman

NASA Ames Research Center
Mofett Field CA 94035-1000

This paper discusses the development of a process to generate a CFD database for the non-linear loads process capability for critical loads evaluation at Boeing Long Beach. The CFD simulations were performed for wing/body configurations at high angles of attack and Reynolds numbers with transonic and elastic deflection effects. Convergence criteria had to be tailored for loads applications rather than the usual drag performance. The time-accurate approach was subsequently adopted in order to improve convergence and model possible unsteadiness in the flowfield. In addition, uncertainty issues relating to the turbulence model and grid resolution in areas of high vortical flows were addressed and investigated for one of the cases.

Outline

This chart gives the outline of the various topics covered in this presentation.

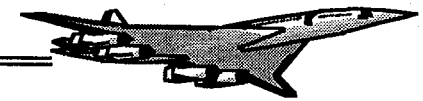

Outline

- Background
- CFD Approach for the M2.4-7A
- Problems encountered
- Convergence criteria
- Time-accurate simulation
- Application to the TCA configuration
- Sensitivity study by NASA Ames
- Conclusion

Background

The current NASTRAN process for generating structural loads is based on linear aerodynamics (Doublet Lattice and ZONA) and the critical load conditions must be supplied by the user. A new process has been developed (Local Equivalence Nonlinear Loads Process shown in the flow-chart below) that provides for a nonlinear loads capability in addition to providing a critical loads selection process. This nonlinear loads process uses a fairly small nonlinear aerodynamic database to correct the linear loads process. The database can either be generated using CFD (in which case representative elastic deflections are used) or from wind-tunnel data (in which case a rigid configuration is used); however, only the CFD approach is described here. All of loads cases (not just the critical ones) can then be easily corrected using this procedure and a new set of high-fidelity critical loads selected and used for structural sizing.

The work to be described here pertains only to the generation of the nonlinear aerodynamic database using CFD. High angles-of-attack and Reynolds numbers, plus transonic and elastic deflection effects, pose special challenges in generating this database. Also, the convergence criteria must be tailored to loads rather than the usual aerodynamic performance.

Initially, the only configuration for which an extensive validated CFD database at transonic regimes was available was the M2.4-7A Opt5 (obtained from nonlinear optimization on the baseline arrow wing). Consequently, the current approach used the later configuration to develop the CFD process for loads applications. Afterwards, the process was applied to the TCA configuration.

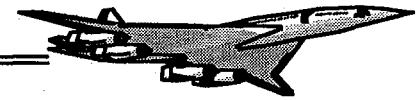

Background

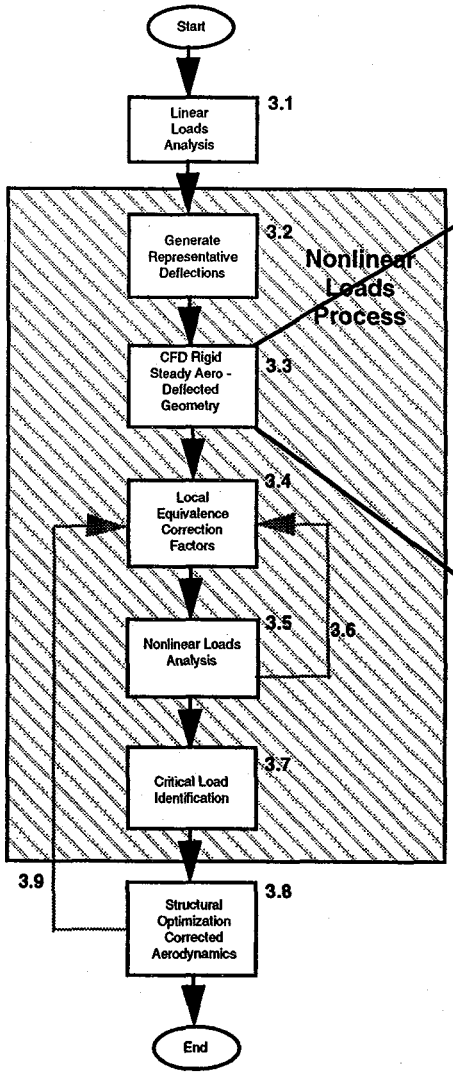

❑Objective:

- Develop process to generate a CFD database for use in the local equivalence correction procedure for the nonlinear loads process

❑Approach:

- M2.4-7A: Learning Process
- TCA application

CFD Approach for the M2.4-7A Configuration

Most of the process development was done with the M2.4-7A wing/body configuration. The optimized M2.4-7A Opt5 configuration was selected because of the extensive validation work done on it under Configuration Aerodynamics (Tasks 3 & 32). Five wing/body configurations were obtained, each corresponding to representative deflections discussed earlier. These configurations correspond to the deflected wing/body shapes as a result of the loads at a given angle-of-attack.

CFD analyses were performed for a single Mach number during the methods development phase of this task. Analysis was done at Mach 0.6 for five representative angles-of-attack ranging from -14° to 23°. The grid consisted of a single-block C-O topology with 93 points in the spanwise direction, 237 in the streamwise, and 89 in the normal directions. The Euler grids for the configurations with representative deflections were generated by perturbing the baseline rigid wing/body grid using a package (CSCMDO) acquired from GEOLAB at NASA Langley. After perturbation, the grids were manually improved and then clustered for Navier-Stokes analyses.

The CFL3D code was used for the N-S analyses. The numerical scheme consisted of flux-difference splitting with multigrid acceleration. The flow was assumed to be fully turbulent and the Baldwin-Lomax algebraic turbulence model with the Degani-Schiff option was used. The Reynolds number used for the simulation was the flight Reynolds number of 301 million (based on the mean aerodynamic chord).

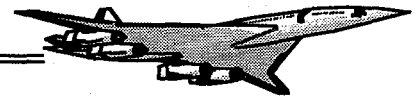

CFD Approach for the M2.4-7A Configuration

❑Configuration:

M2.4-7A Opt5 wing/body

❑Grid-Topology:

C-O grid of 93x237x89

❑Geometries:

Obtained from deflected shapes for cases ranging from -1g to 2.5g at five angles-of-attack

❑Grid Generation:

Perturbation of a rigid baseline Euler grid (CSCMDO/FLEXMESH) and clustering for N-S

❑Analysis:

CFL3D N-S, steady flow, Baldwin-Lomax turbulence model (Degani-Schiff option turned on for higher angles-of-attack)

❑Flight Conditions:

Mach= 0.6, Re_c= 300 million. angles-of-attack of -14, 1.8, 12, 18, and 23 degrees

M2.4-7A Opt5 Wing/Body Shapes

The chart below shows two of the geometries used for the CFD analyses. The rigid geometries are shaded while the C-O grid topology is shown for the deflected shapes. The figures below show the wing/ body configuration with the fuselage attached to a wind-tunnel sting. Note that the fuselage is also structurally deflected.

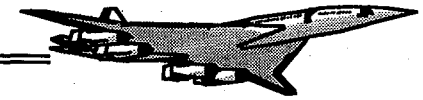

M2.4–7A OPT 5 Wing/Body Shapes

Baseline and Deflected Configurations for the Database

α= –14°

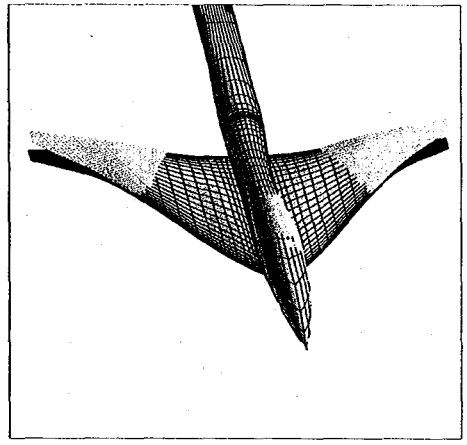

Front View

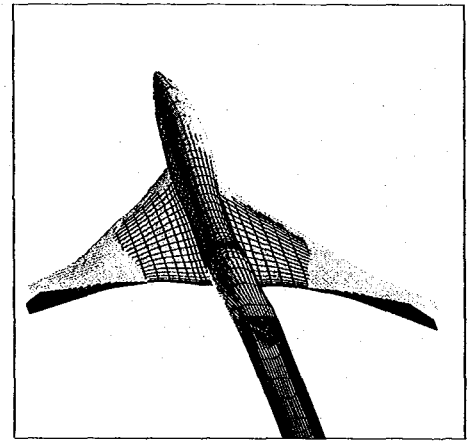

BackView

α= 23°

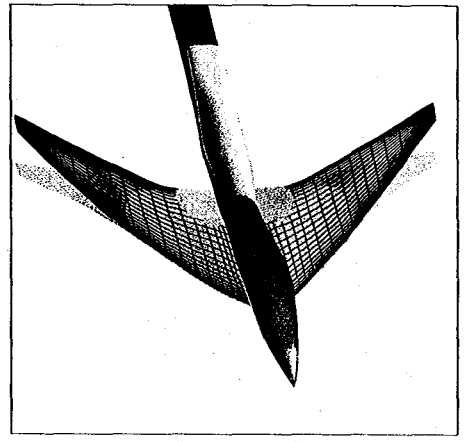

Front View

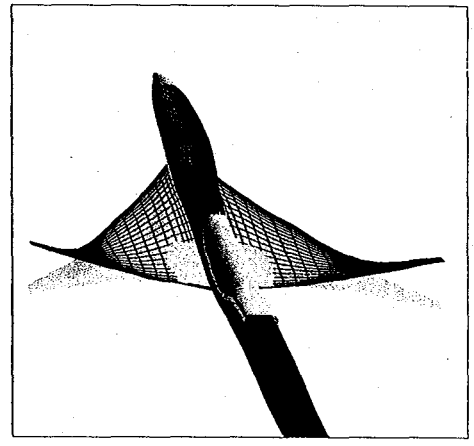

BackView

BOEING

Convergence History for the M2.4-7A Opt5

When the steady-state formulation in CFL3D is used for the higher angles-of-attack, the solution does not converge smoothly. For example, the solution for the representative geometry corresponding to the 22.9° angle-of-attack is shown above. The residual seems to "hang up" with lift and drag fluctuating in a range of 4 to 5%. The reason for this fluctuation is believed to be the highly separated flow with separation lines coincident with the strong vortices formed at the nose and wing apex.

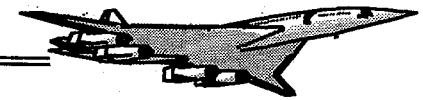

Convergence History for M2.4-7A Opt5 Configuration with Deformation

CFL3D N-S (B-L, D-S); $Re_c=301x10^6$; M=0.60; α=23.050°; C-O(93x237x89)

(2 Level Multigrid; Integration w/ full sting)

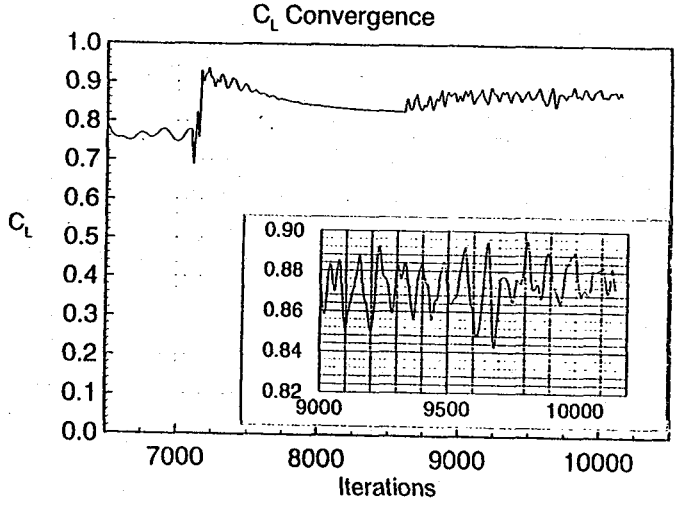

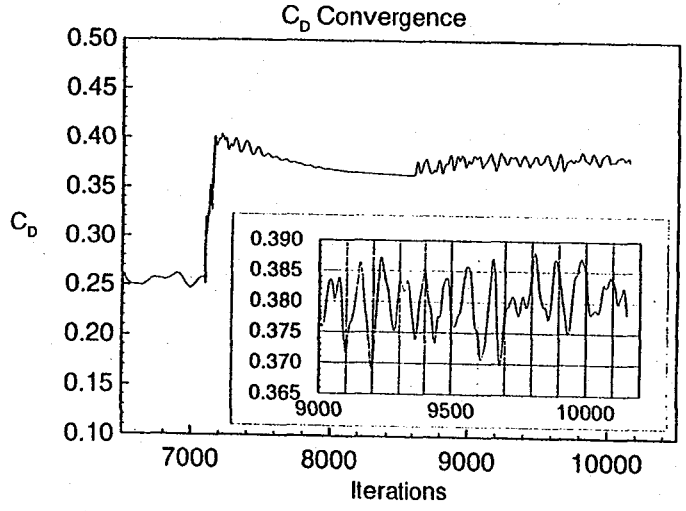

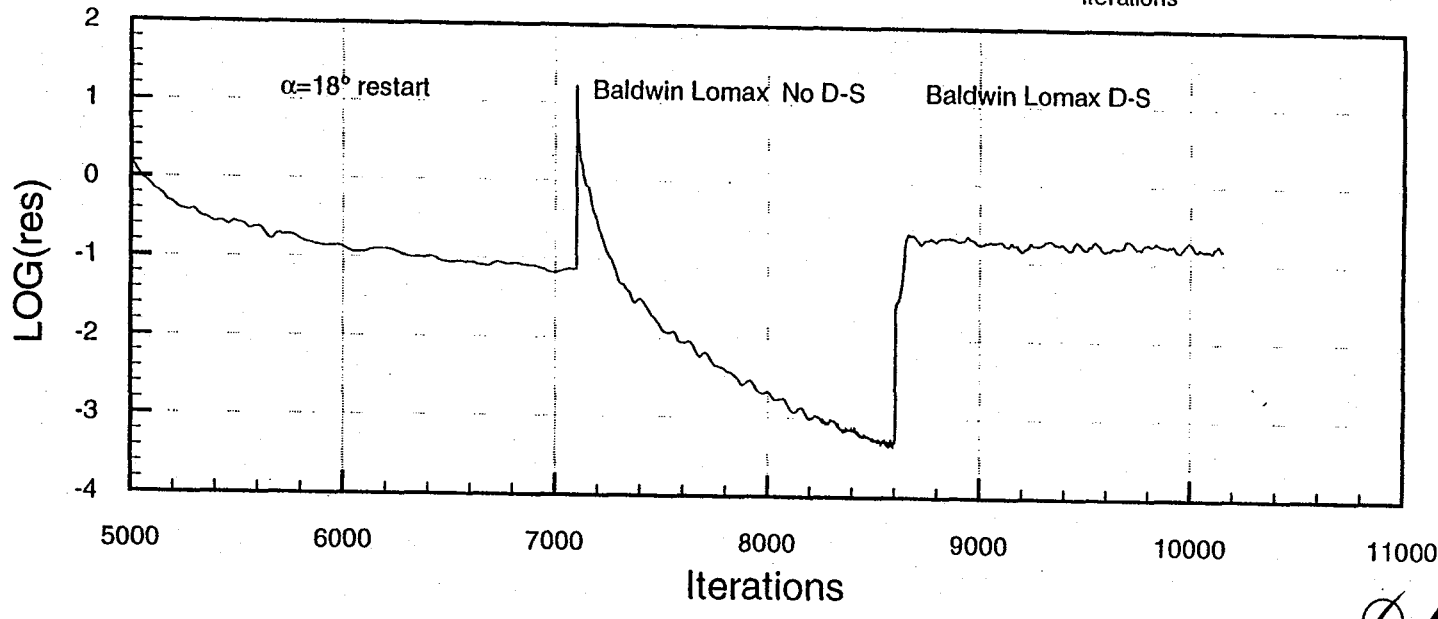

BOEING

M2.4-7A Opt5 W/B Surface Flow Traces

The surface streamlines at the end of 10,100 iterations are shown in the figure on the left. There is an indication of flow separation on the upper surface which is most likely contributing to the unsteadiness in the solution.

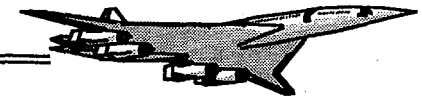

M2.4–7A Opt5 W/B Surface Flow Traces

CFL3D N–S, 10100 Iterations, M_∞=0.6, α=23.05°

$Re_c = 301 \times 10^6$

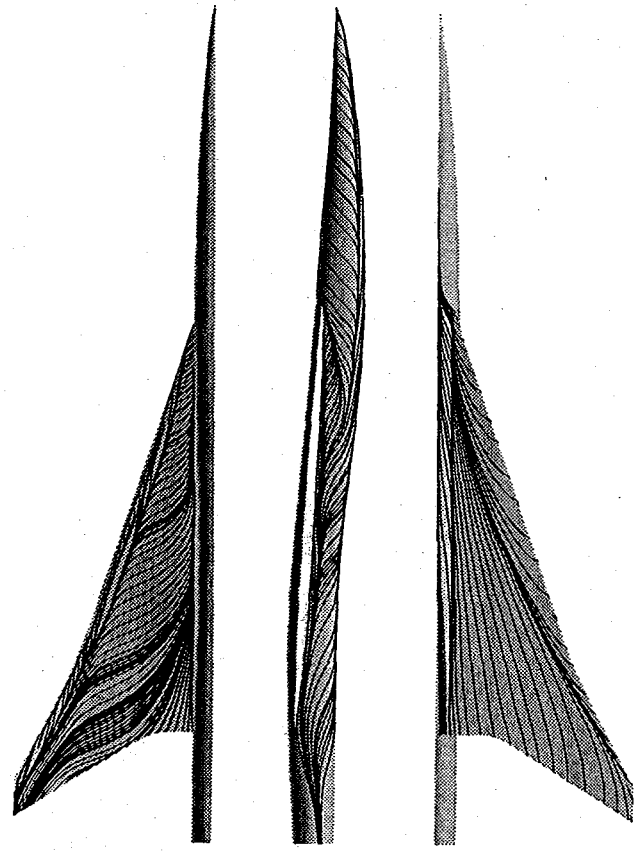

Top View Side View Bottom View

BOEING

Convergence Summary for the Opt5 Wing/Body

The two plots below, correspond to the -14° angle-of-attack case. The figure on the left hand side shows the sectional lift (scaled by the total lift coefficient at a given iteration) for the last 100 iterations. The values show a significant scatter. The figure on the right shows the axial location of the center-of-pressure X_{cp} as a function of span. This plot indicates that the X_{cp} varies significantly over the outboard wing. Since these results indicate a lack of convergence, new criteria need to be developed in order to establish convergence for CFD solutions in support of non-linear loads.

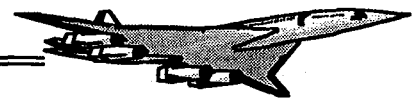

Convergence Summary for M2.4-7A Opt5 Wing/Body Wing with Representative Deflections

CFL3D N-S, M_∞=0.60, α=-14.0 deg., Re/ft=3.21 million, 93x237x89 C-O Grid

$XC_{P,i}$ = Local Center-of-Pressure at Iteration "i"

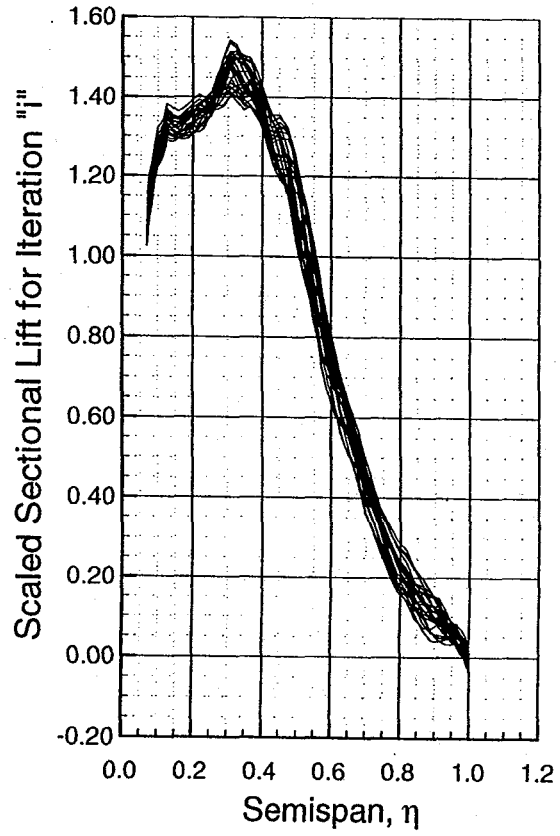

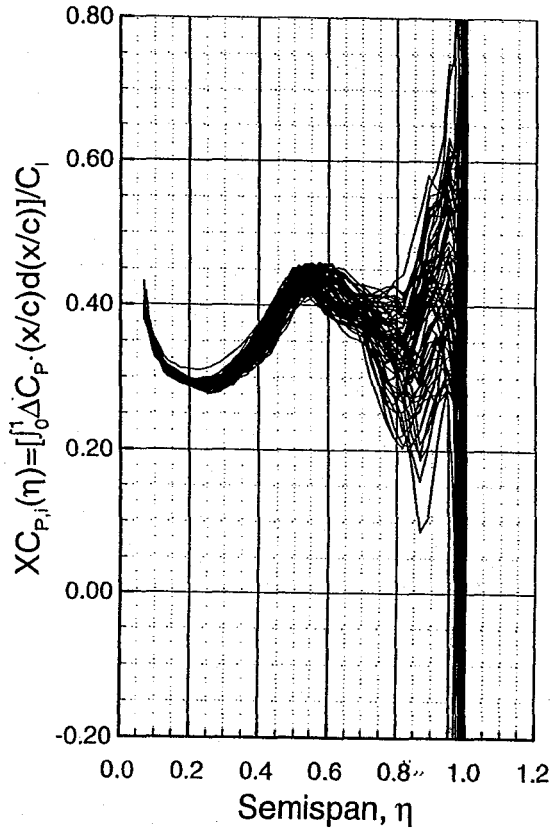

BOEING

Convergence Criteria for Loads

Convergence criteria were established by monitoring several quantities of interest:

(a)- The "mean" lift coefficient (integrated over wing/body) and its % deviation. The mean value is computed by a "moving average" technique. In other words, the values of C_L are averaged over the total number of iterations as the solution progresses, with an update every 10 iterations. This is a useful parameter, but the % deviation could become quite large when the mean value approaches zero.

(b)-The actual value of the fluctuation between the latest available peak and trough is computed.

(c)-The spanwise distributions of the sectional lift and center-of-pressure are also monitored at each iteration. The sectional loads (cC_l/c_{bar}) are scaled by C_L at each iteration to give insight not only on the magnitude of the fluctuation but also on shape changes (i.e., spanwise shifting of the load).

(d)-The variations in the quantities of interest were quantified by the use of σ and ε, which are the respective rms values of the difference between the scaled sectional loads and center-of-pressure curves at local peaks and troughs.

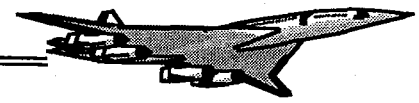

Convergence Criteria for Loads

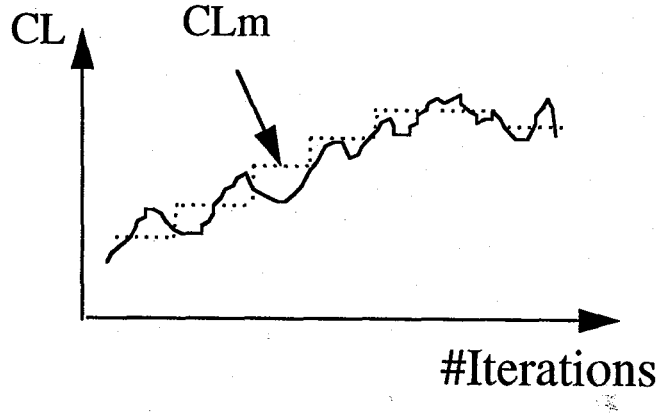

- % Deviation from mean (moving average):

$$(CL_n - CL_m)/CL_m$$

- Difference between peaks & troughs:

$$\Delta(C_L) = | CL_p - CL_t |$$

- Non-dimensional sectional lift:

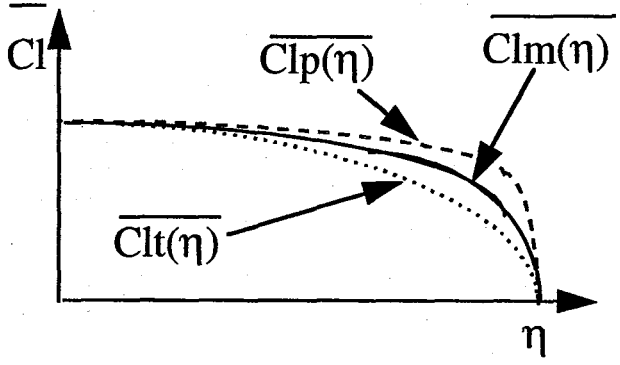

$$\overline{Cl}(\eta) = \left(\frac{cCl}{\bar{c}}(\eta)\right)_i \Big/ CL_i$$

- Mean values of the relevant shape variations:

$$\sigma = \sqrt{\int_0^1 (Cl_p - Cl_t)^2(\eta)\,d\eta}$$

- Similar approach for the center-of-pressure

BOEING

Convergence Summary for the Opt5 Wing/Body

The figures below show the convergence criteria applied to the $\alpha = -14.0^\circ$ case. The lift quantities monitored, are varying within 2 to 5% of the respective mean values.

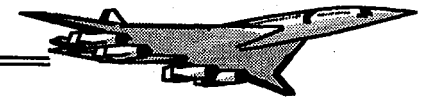

Convergence Summary for M2.4-7A Opt5 Wing/Body Wing with Representative Deflections

CFL3D N-S, M_∞=0.60, α=-14.0 deg., Re/ft=3.21 million, 93x237x89 C-O Grid

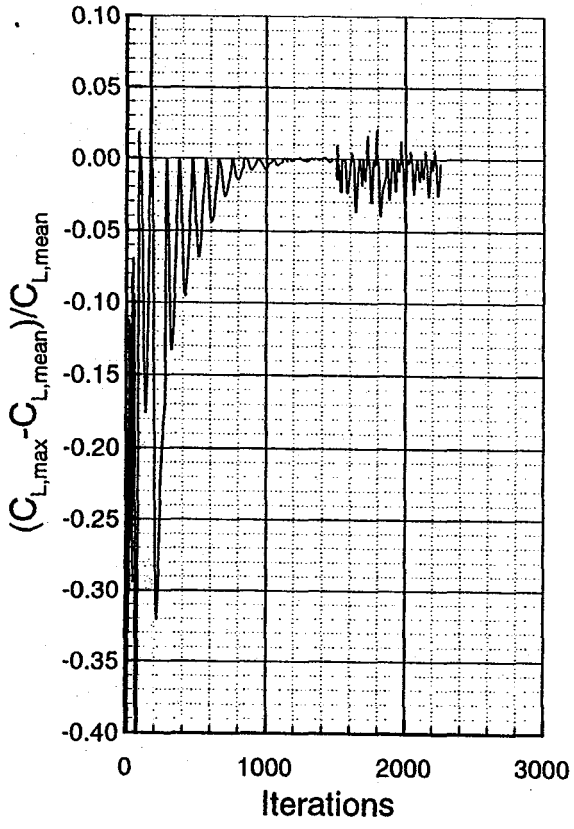

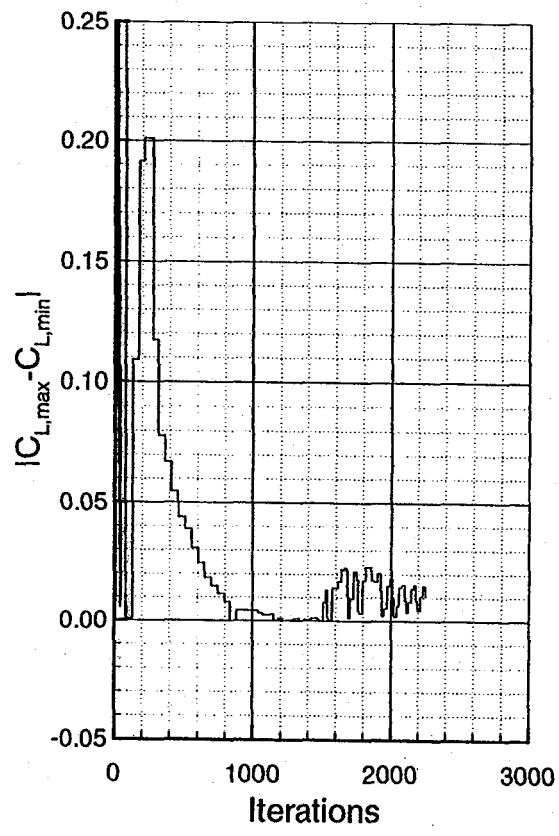

BOEING

Convergence Summary for the Opt5 Wing/Body

The figures below show the convergence criteria applied to the α= -14.0° case. The sectional loads quantities monitored, are varying within 2 to 3% for σ and 5 to 8% for ε. Consequently, the large variations of the sectional loads and X_{Cp} curves observed are reflected in the monitored quantities. These fluctuations reflect flow unsteadiness patterns that are either numerically induced or actual features of the highly separated flowfields.

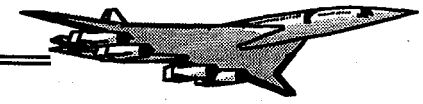

Convergence Summary for M2.4-7A Opt5 Wing/Body Wing with Representative Deflections

CFL3D N-S, M_∞=0.60, α=-14.0 deg., Re/ft=3.21 million, 93x237x89 C-O Grid

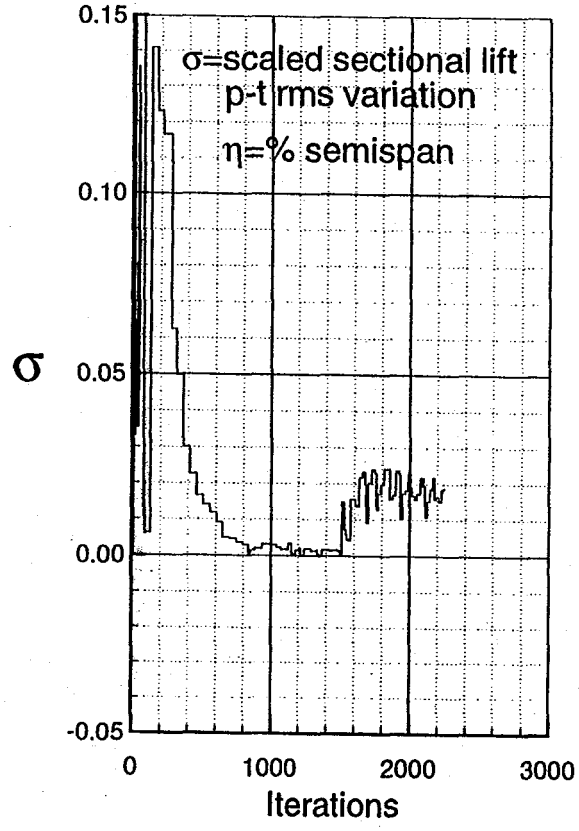

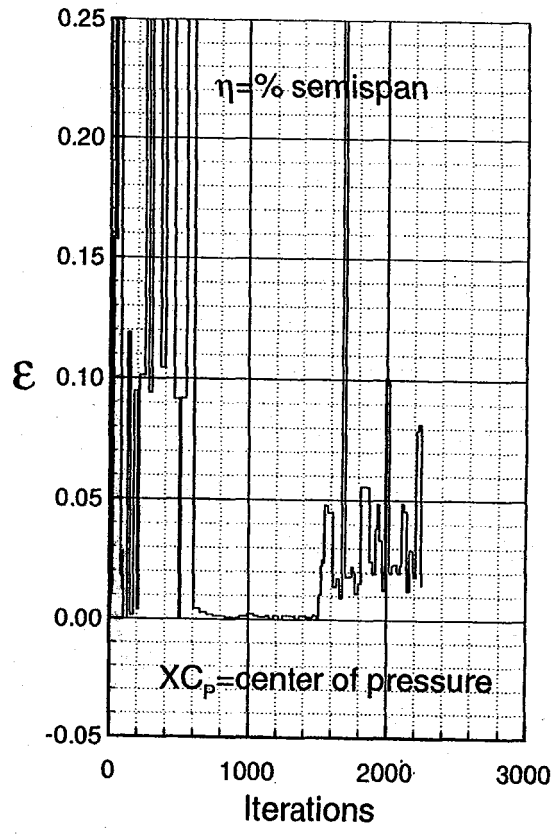

BOEING

Time-Accurate Simulation

The answer to the question of numerical vs. flowfield unsteadiness can be provided by a time-accurate simulation. In fact, the time-accurate analysis to perform the steady high angle-of-attack simulations was suggested by Scott Murman and Neal Chaderjian from NASA Ames based on their experiences with delta wings and F-18 flight tests.

The $\alpha = -14^\circ$ case was used as a test-bed for the time-accurate simulations because of its particular "lack" of convergence. The time-accurate approach used with the implicit scheme present in CFL3D consisted of the τ-TS second- order-in-time method. The use of three sub-iterations per time-step allowed the lowest computational cost (the code manual recommended five). In this case, each time-accurate step will be equivalent to 3 steady-flow iterations. It was estimated that the flowfield can be covered by 1000 time-steps which yields a non-dimensional time-step of 11.25 (~ 0.001 sec). The time-accurate solutions assume a pseudo-time CFL of 10.

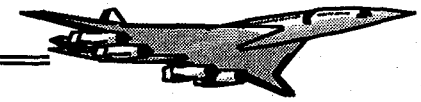

Time-Accurate Simulation

- Restart from steady-state solution: α = -14 deg.
- Approach:
  - τ-TS method
  - 3 subiterations
  - Estimated # of iterations to cover flowfield ~ 1000 → dt= 11.25
  - Attempts to increase time-step
- Improved overall convergence with a 20-30% increase in CPU cost

Convergence History for Opt5 with Deformation

The figure below shows the convergence history before and after the use of time-domain computations. The overall residual seems to monotonically decrease once the time-accurate mode is initiated at iteration #5600 and the amplitude of C_L oscillation went down by about an order of magnitude. However, the use of a larger time-step did not seem to help the convergence with the given number of sub-iterations.

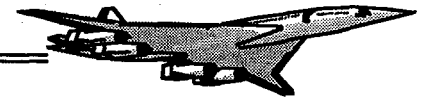

Convergence History for M2.4-7a Opt5 Configuration with Deformation

CFL3D N-S (B-L, D-S); Re_c=301x10^6; M_∞=0.60; α=-14.565°; C-O(93x237x89)

(2 Level Muligrid; Integration w/ full sting)

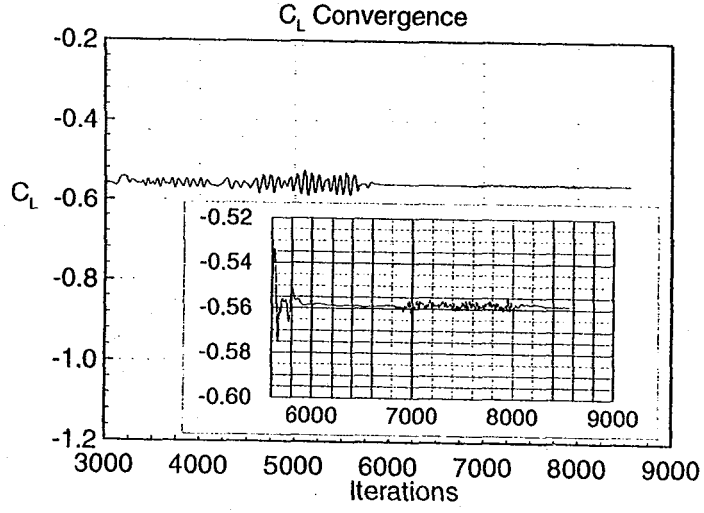

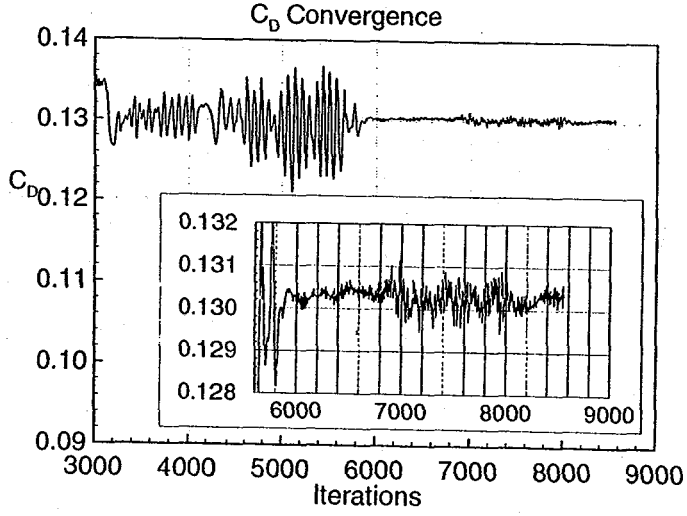

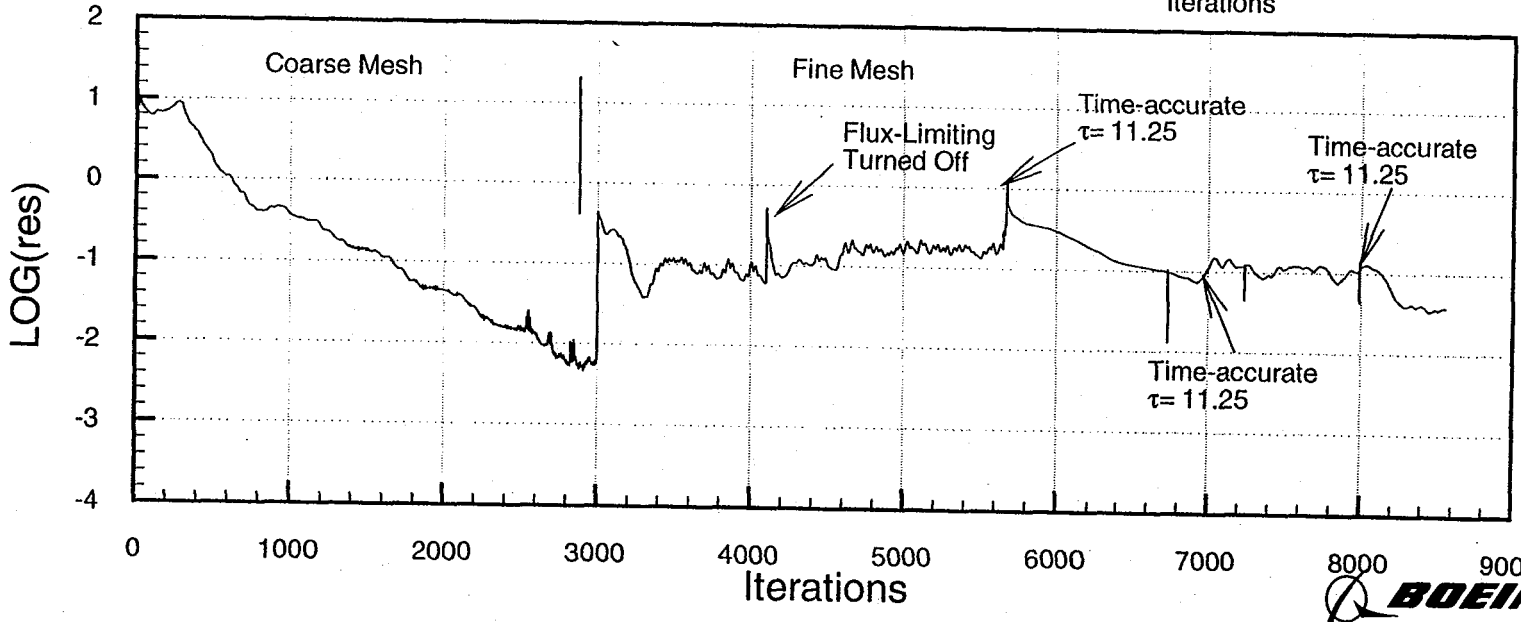

BOEING

Loads Calibration Study, Sectional Lift

As shown in the figure below, the decrease in oscillations was also seen at the sectional load level, the amplitude of oscillations around a mean curve has been significantly reduced. In fact, very little difference is observed between the time-accurate peak and trough curves.

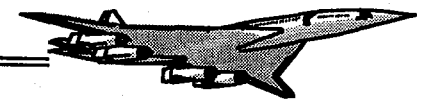

Loads Calibration Study, Sectional Lift
M2.4-7A Opt5 W/B Configuration with Deformations

CFL3D N-S (B-L,D-S); $Re_c = 301 \times 10^6$; $M_\infty = 0.6$; $\alpha = -14.565^\circ$; C-O (93x237x89)

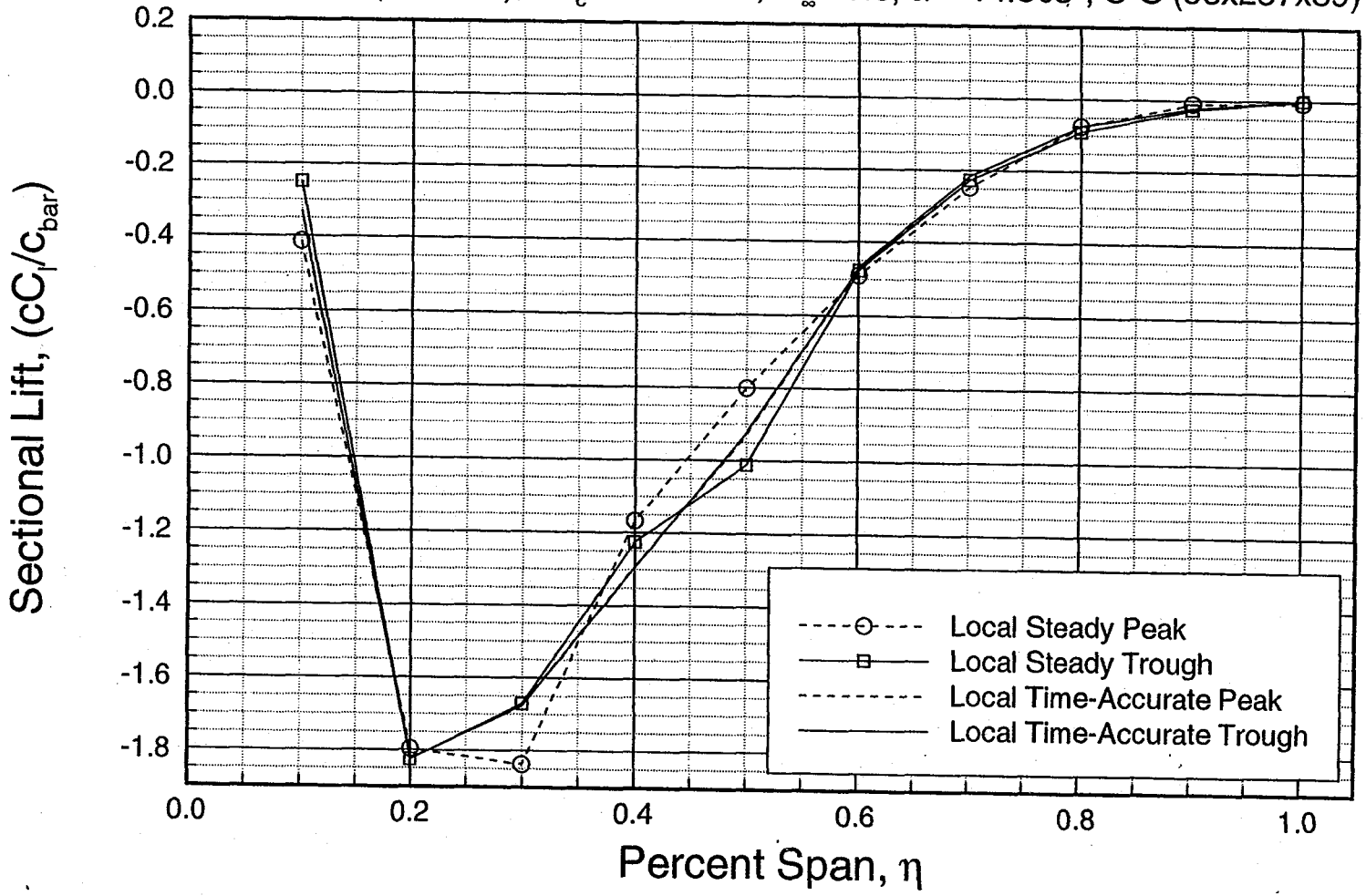

BOEING

Lessons Learned from CFD Analysis of M2.4-7A

When clustering the CFD grids for the deflected shapes (obtained from perturbation of the rigid baseline grid) for the flight Reynolds number (about 300 million), many problems were encountered and manual improvement of the grid quality was needed. Consequently, the use of a lower Reynolds number (~40 million for example) was suggested to simplify the grid generation process.

The flowfield at higher angle-of-attack is very unsteady and no particular periodicity of the monitored quantities for convergence was observed. Due to the complex flow mechanism at high angles-of-attack, steady-state equations are inadequate and time-accurate solutions are needed.

Special convergence criteria have been established for loads calculations. Quantities, such as spanwise lift, its rms fluctuation from peak to trough, and fluctuation from mean of the total lift coefficient, are monitored for convergence. These convergence criteria are better suited for CFD loads analysis, as opposed to those used in typical attached flow cases normally encountered for aerodynamic performance (e.g., drag).

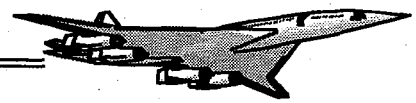

Lessons Learned from CFD Analysis of M2.4-7A

- Grid generation must be simplified (use of flight Reynolds numbers created highly clustered grids)
- Very unsteady-like behavior for higher angles-of-attack, no particular periodicity
- Need special loads convergence criteria
- Steady-state equations inadequate, need time-accurate solutions

Application to the TCA Configuration

The approach for the TCA configuration was similar to that used for M2.4-7A with the exception that the grid was preprocessed for both leading and trailing-edge flaps. Here, the C-O topology used more points in the streamwise direction and a smaller number of points in the viscous direction. The process that takes a clean wing/body grid and does the actual flap deflection and relevant grid perturbation has been developed and validated in the high-lift group under HSR Task 33 (High-Lift). The rigid configuration, had the outboard leading-edge flaps deflected by 8° to represent the range of Mach numbers, since the generation of the grid for different flap settings for every Mach number would require considerably more effort. The grid perturbation process for the deflected shapes has been improved significantly and fewer difficulties were encountered than for the M2.4-7A grid. In order to ease the clustering and facilitate convergence it was decided to use a lower Reynolds number of 40 million. The expectation is that the solution based on a Reynolds number of 40 million would be adequately representative of the full-scale flowfield. However, additional work on this topic is being done by NASA Ames and is reported in section 4.7. As in the M2.4-7A arrow wing, the CFL3D N-S code with the Baldwin-Lomax (Degani-Schiff) turbulence model was used. Based on the M2.4-7A experience, it was decided to use the time-accurate mode of analysis with the established convergence criteria for all cases. Since the grid used was three-level multigridable, steady-state solutions with coarse and medium meshes were obtained first and time-accurate simulations were started with the very first iteration of the fine grid (with a few exceptions).

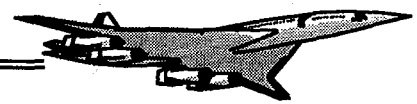

Application to the TCA Configuration

- **Configuration:**
  - TCA wing/body
- **Grid-Topology:**
  - C-O grid of 93x281x69
- **Geometries:**
  - Obtained from representative deflections
- **Grid Generation:**
  - Preprocess for flaps / flap deflection
  - Perturbation of a rigid baseline Euler grid (CSCMDO) and clustering for Navier-Stokes analyses
- **Analysis:**
  - CFL3D N-S, time accurate, Baldwin-Lomax turbulence model (Degani-Schiff option turned on for higher angles-of-attack)
  - Reynolds number of 40 million (based on the mean aerodynamic chord)

Cases Analyzed

The simulations were performed at four different Mach numbers, 0.8, 1.2, 2.0, and 0.95 in increasing order of difficulty. The five angles-of-attack were -10.5, 2.83, 12.11, 18.3, and 22.9°. However, only Mach 0.8 included the 23° case and Mach 2.0 did not include the 18 deg. case. Consequently, four cases were eliminated. The table below shows the flow conditions and angles-of-attack that were analyzed for the TCA wing/body/LE flap configuration. Among the matrix of 20 cases to run four cases were omitted. It was decided that computations at an angle-of-attack of 23° will not be necessary for the nonlinear loads database at Mach numbers above 0.95. As a matter of fact, even the 18° angle-of-attack case was not necessary for Mach 2.0.

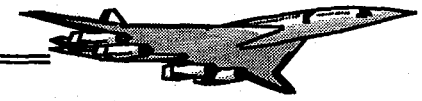

Cases Analyzed

	Deflected Shape				
	α= -10.4 °	α= 2.83 °	α= 12.1 °	α= 18.3 °	α= 22.9°
Mach 0.8	✔	✔	✔	✔	✔
Mach 1.2	✔	✔	✔	✔	N/A
Mach 0.95	✔	✔	✔	✔	N/A
Mach 2.0	✔	✔	✔	N/A	N/A

Flow Analysis of the TCA Wing/Body/LE Flap

An example of a benign (low α) transonic flowfield (α=2.83°, M_∞= 0.95) is shown in the chart above. The left side of the figure shows the normalized total pressure cuts along several span stations while the right side displays the surface pressure coefficients on the wing with field streamlines. The flow is benign as expected and no separation pattern is observed. In spite of the higher spanwise component of the streamlines near the tip, significant flow acceleration/expansion is observed along the flap edge.

Flow Analysis of the TCA Wing/Body/Leading–Edge Flap Configuration with Representative Deflections Streamwise Total Pressure cuts, Surface Cp Distributions and Streamlines

CFL3D, N–S, Baldwin–Lomax D–S, M_∞= 0.95, α= 2.83°, Re_c= 40 million

(C–O Grid 93x281x69)

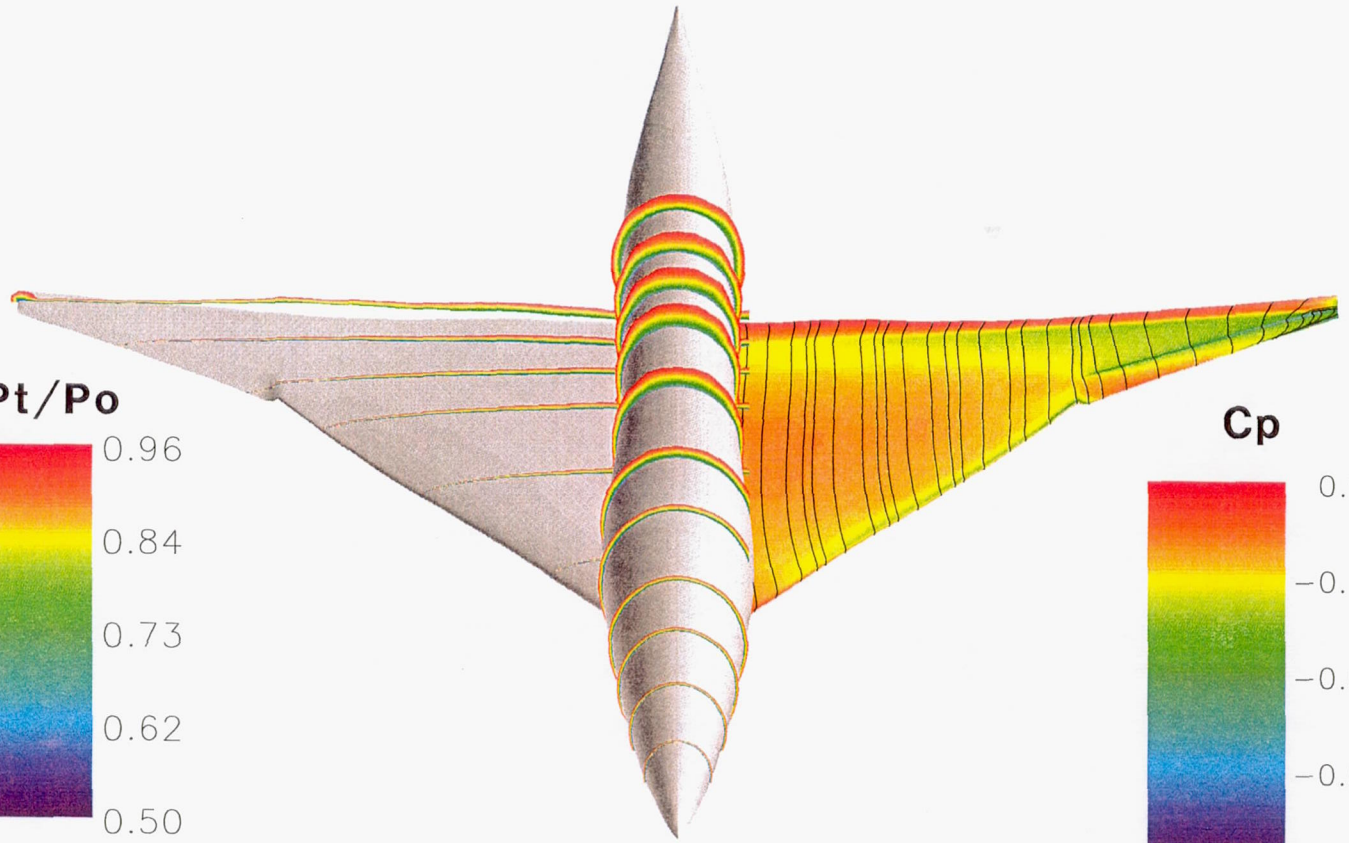

BOEING

Flow Analysis of the TCA Wing/Body/LE Flap

The flowfield for this negative angle-of-attack case (α=-10.44°, M_∞= 0.95) is not as benign as shown in the figure below. The left side of the plot indicates three types of vortices. The first one would be the forebody vortex which remains significant up to the wing trailing edge. The second type of vortex gets started at the wing apex and dominates the wing lower surface flowfield. When examining streamwise cuts from the apex, a secondary vortex is observed starting at the sixth streamwise cut from the wing apex. This flow feature cannot be captured without the use of the Degani-Schiff option in the turbulence model. The third type of vortex is the wing leading-edge break vortex which tends to be stronger because of the 8° outboard leading-edge flap deflection.

Flow Analysis of the TCA Wing/Body/Leading–Edge Flap Configuration with Representative Deflections

Streamwise Total Pressure cuts, Surface Cp Distributions and Streamlines

CFL3D, N–S, Baldwin–Lomax D–S, M_∞= 0.95, α=–10.44°, Re_c= 40 million

(C–O Grid 93x281x69)

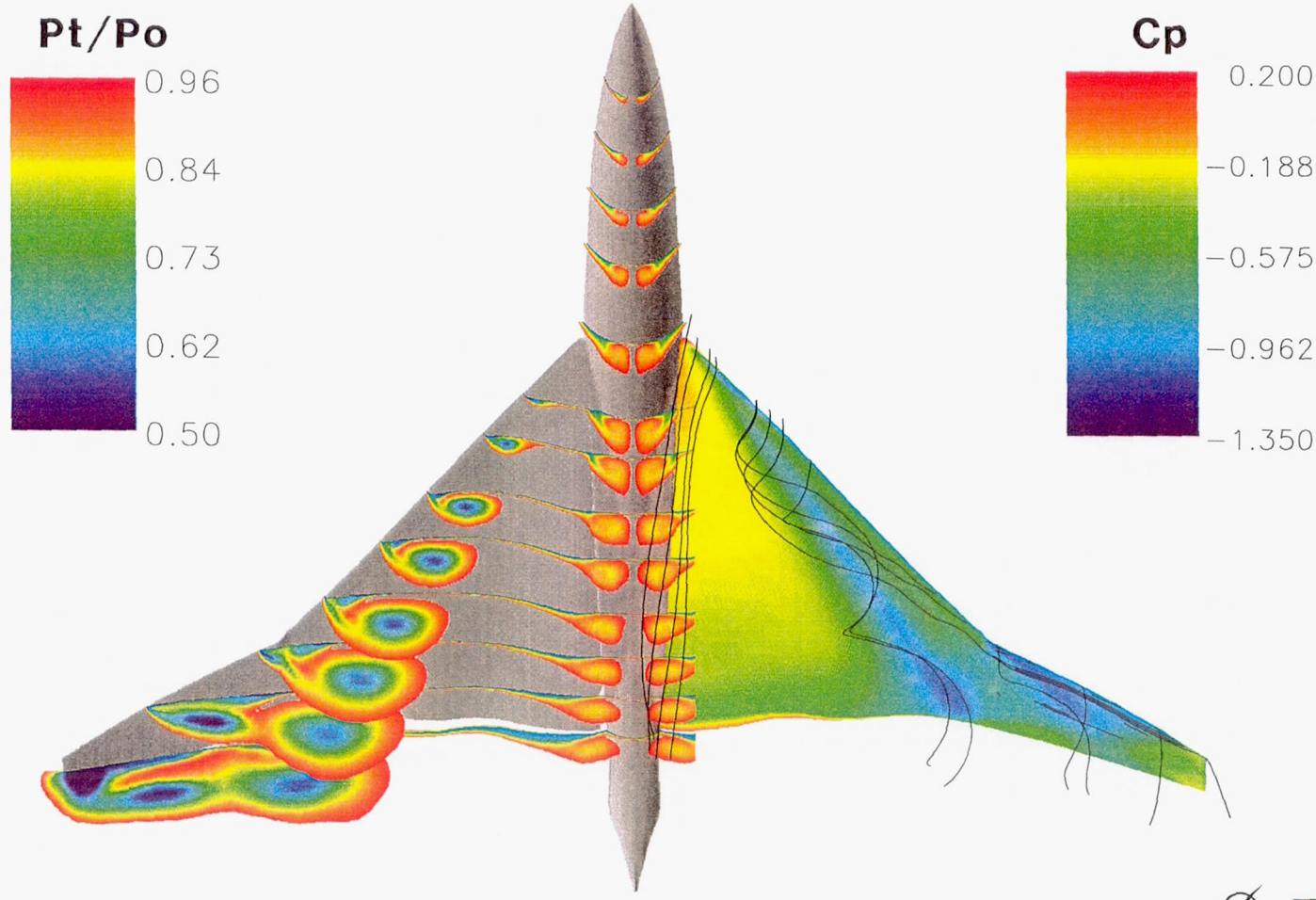

BOEING

Flow Analysis of the TCA Wing/Body/LE Flap

The flowfield for the 18.3° angle-of-attack at Mach 0.95 case is shown in the figure below. Here, the forebody vortex bursts halfway through the fuselage since the upper surface vortex interactions with the fuselage causes the vortex to burst sooner. The wing upper surface pressure contours show a "shadow" of the apex vortex. When looking at the fifth streamwise normalized total pressure cut from the wing apex, three types of vortices are observed. The main apex vortex is followed by a secondary vortex at the verge of bursting. Finally, the leading-edge break vortex moves away from the surface allowing the wing-tip vortex to be seen at the last cut. For these higher positive angle-of-attack cases, higher Mach numbers show similar results. Also, vortices tend to be flatter with higher Mach numbers.

Flow Analysis of the TCA Wing/Body/Leading–Edge Flap Configuration with Representative Deflections

Streamwise Total Pressure cuts, Surface Cp Distributions and Streamlines

CFL3D, N–S, Baldwin–Lomax D–S, M_∞= 0.95, α= 18.3°, Re_c= 40 million

(C–O Grid 93x281x69)

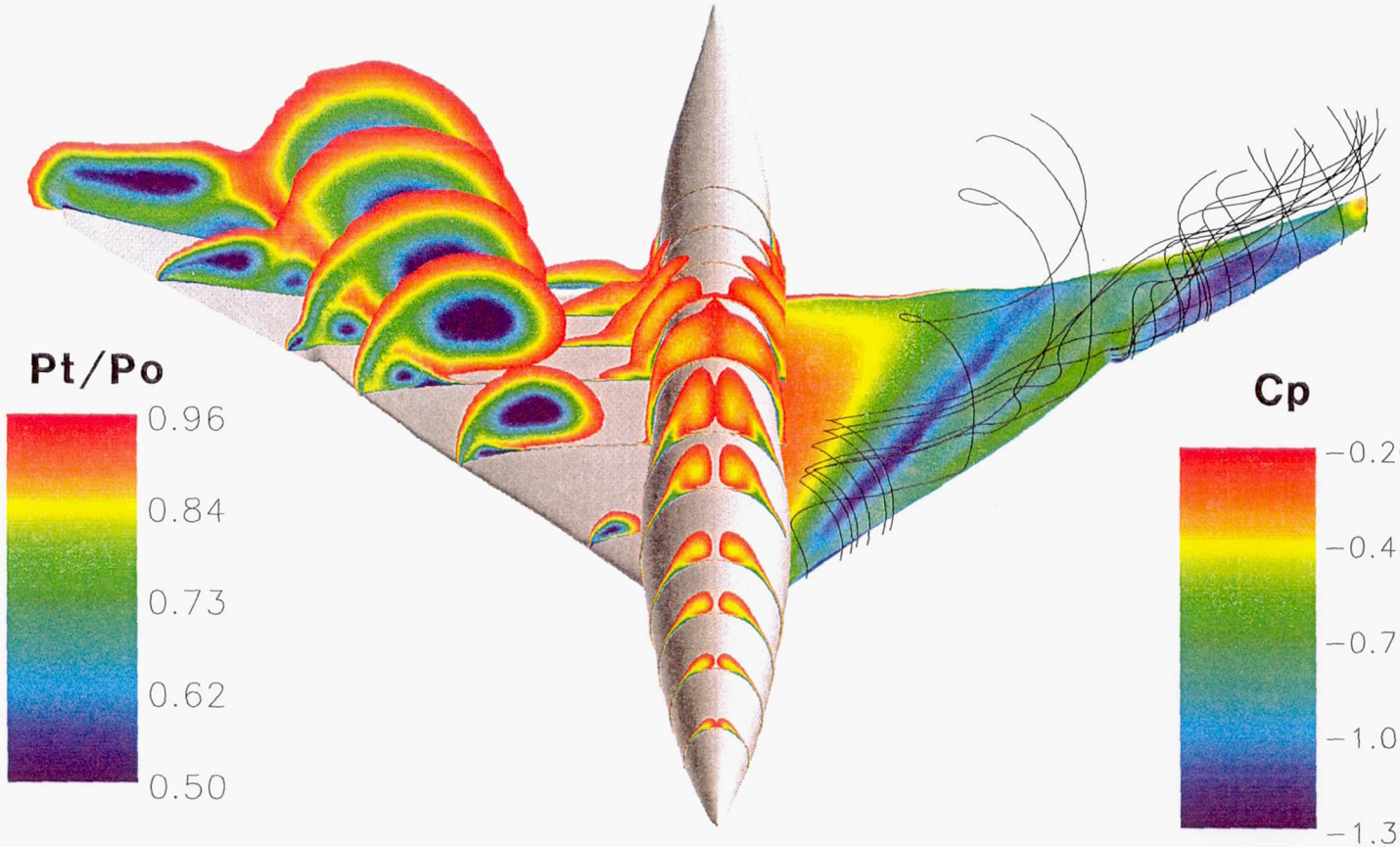

BOEING

Convergence History for the TCA W/B/LE Flap

Convergence results for the 18.3° at Mach 0.95 case are shown in the figure above. This is one of the most difficult case to converge. In fact, when looking at the residual history, more iterations were needed for this case. Lift and drag had one last oscillation of 0.1%.

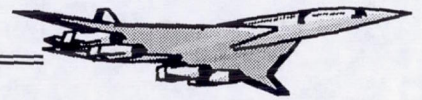

Convergence History for the TCA W/B/LE Flap Configuration with Deformation

CFL3D N-S B-L D-S; $Re_c=40x10^6$; M=0.95; $\alpha=18.3°$; C-O(93x281x69)

(3 Level Multigrid; Integration w/ full sting)

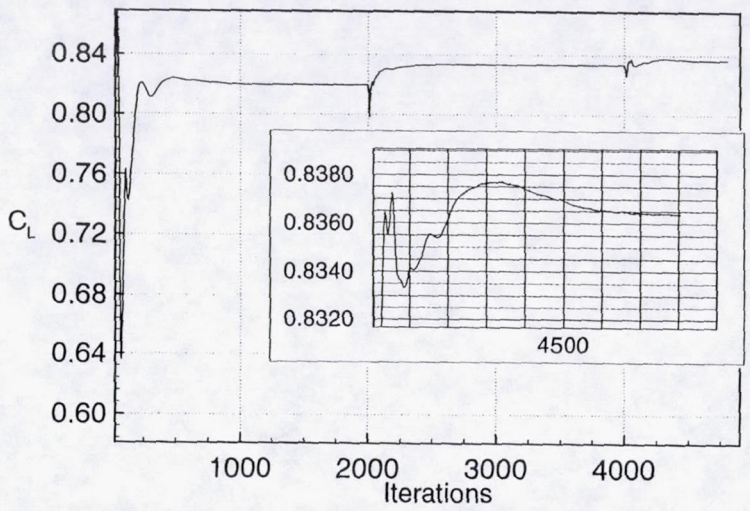

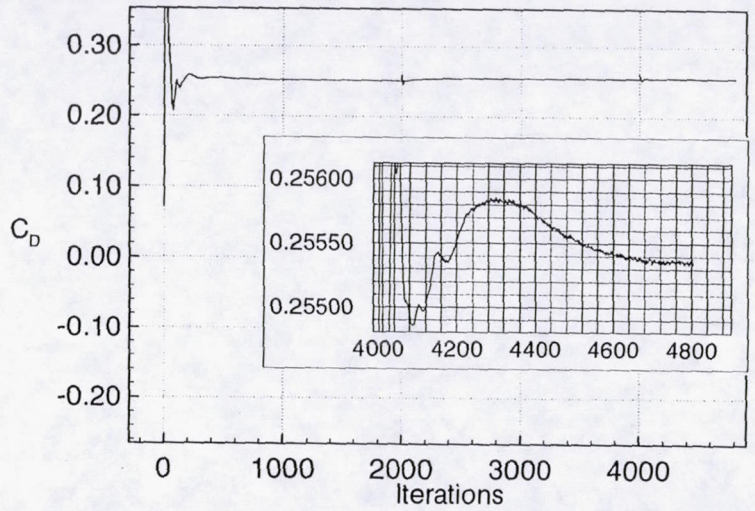

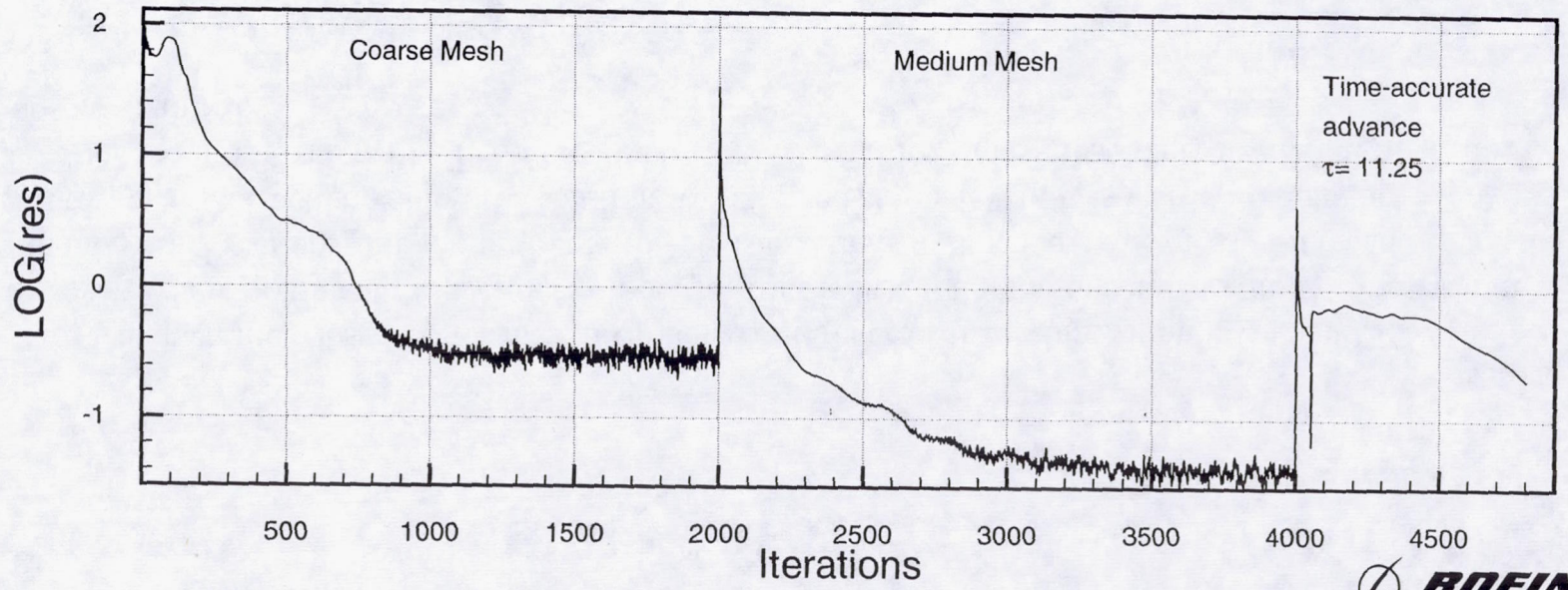

BOEING

Convergence Summary for the TCA W/B/Out LE Flap

The quantities observed for the convergence criteria are all varying within less than 0.1%. However, when looking at the sectional properties for the last 200 iterations no variation is observed in both the scaled sectional lift and the center-of-pressure curves . Since, the thickness of the band is small with respect to the actual values, the solution was stopped at this level. It is worthy to note that every 565 iterations required 8 hours of CPU time on the C-90. Therefore, unless absolutely needed, further time steps are avoided.

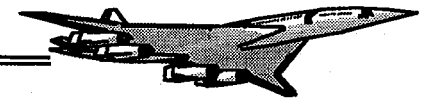

Convergence Summary for the TCA Wing/Body/Out LE Flap Wing with Representative Deflections

CFL3D N-S, Baldwin-Lomax D-S, M_∞=0.95, α=18.0 deg., Re_c=40 million, 93x281x69 C-O Grid

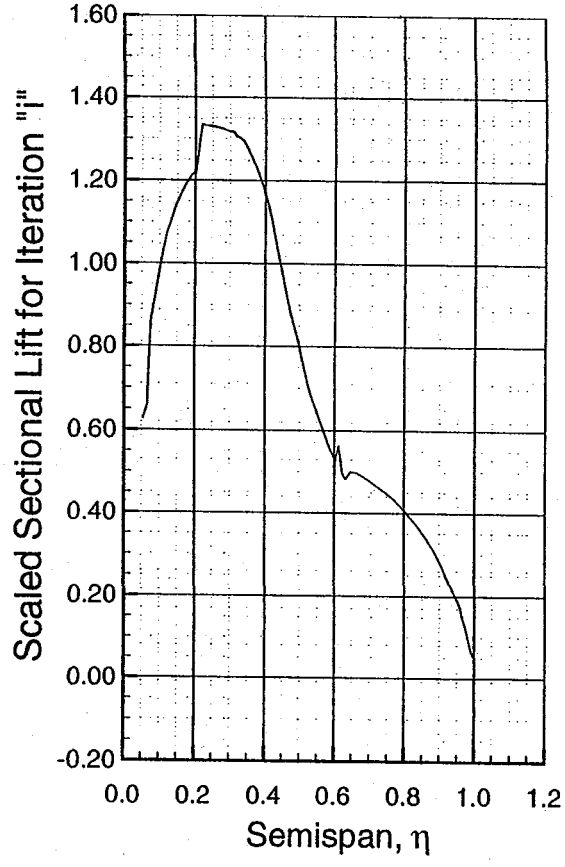

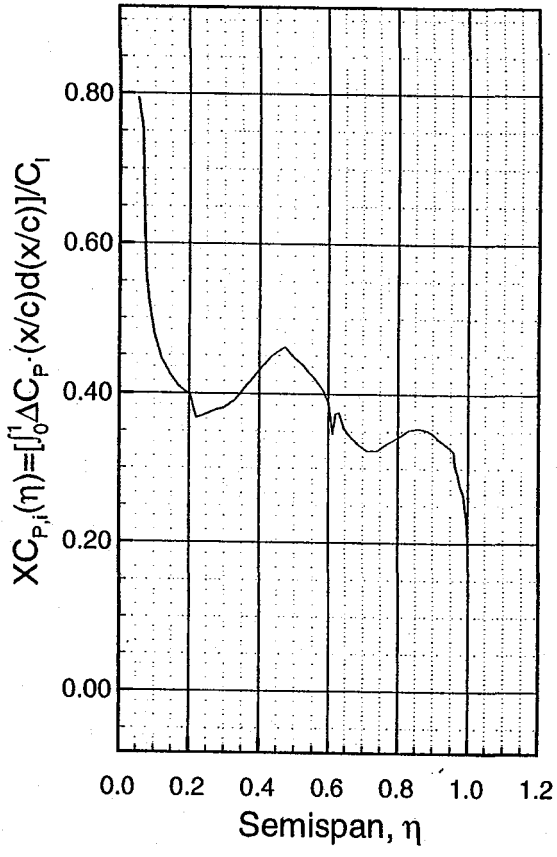

BOEING

Sensitivity Study by NASA Ames

The 18° angle-of-attack case discussed previously did not show significant fluctuations and was actually one of the better behaved cases. Other flow regimes showed much larger fluctuations. In fact, the uncertainties related to the turbulence model effect, grid density and resolution in the areas where strong vortices are formed, and Reynolds number effect, remain to be assessed.

The emphasis here is solely on the loading due to lift forces, and not on the drag forces which would require more sophisticated (and time-consuming) schemes. The loads analysis calculations were all performed on a single configuration at the same flow conditions as the previous three charts. As a first step, the objective of this assessment will address the effect of three main components on loading: effect of turbulence model, resolution of the fuselage forebody, and the density in regions of off-surface vortices. It was attempted to analyze the effects of each of these components individually by computing incremental changes from a baseline configuration. In this way, while it can't be claimed which method is the most accurate (due to a lack of experimental data), the effect of each component investigated, as well as the cumulative effect of all, can be stated in terms of percentage change. The CFD code used for this sensitivity study was OVERFLOW.

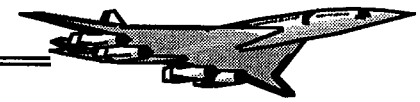

Sensitivity Study By NASA Ames

- **Issues:Uncertainty Assessment by NASA Ames ACE teammates**
  - Turbulence model
  - Grid density/resolution
  - Reynolds number
- **Objective: Assess the influence of the following on the CFD loads prediction for the deflected TCA configuration at α= 18°, M_∞= 0.95, Re_c= 40 million:**
  - Turbulence model (production vs. "True" Degani-Schiff)
  - Forebody grid resolution (effect on forebody vortex)
  - Off-surface, wing vortex grid resolution

Effect of Turbulence Model on Pressure Distributions

The figure below shows the computed surface flow pattern over the wing for two computations with different versions of the Degani-Schiff modification. The blue lines in these figures represent spanwise stations that will be used to examine the wing loading more closely. In both computations, on the inboard wing sections the flow separates from the wing leading edge, reattaches near the wing root, and then induces a boundary layer flow outboard from the wing root. This induced boundary layer separates in a similar manner to a crossflow separation, and reattaches near the leading edge. A tertiary separation is also present between the secondary separation and reattachment lines. Over the outboard section of the wing, the flow again separates at the leading-edge and induces a secondary flow which also separates at about the quarter chord location. Comparing the two turbulence model implementations, the OVERFLOW version has a delayed secondary separation and, in general, a tighter bunching of the secondary/tertiary separation region. The OVERFLOW implementation is predicting a higher value of the turbulent eddy viscosity near the separation locations, which in turn delays the onset of the flow separation. These computations were performed at a freestream Mach number near unity where the flow would form a shock wave near the wing trailing edge. The OVERFLOW implementation is producing a distinct shock-induced separation line near the wing trailing edge, as expected. The modifications which follow, show a more complicated separation pattern near the trailing edge, which does not correspond to a sharp shock wave. It is felt that the logic of the Degani-Schiff modifications as originally reported in Degani's paper (1986), which was designed solely for crossflow separation, is being confused by the streamwise shock-induced separation of this case, and leading to erroneous results. In both implementations of the turbulence model, a complicated flow structure is visible near the wing tip. It is felt that this is a result of unsteadiness in the computations.

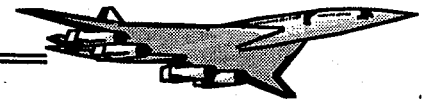

Effect of Turbulence Model on Pressure Distributions and Wing Upper Surface Flow Pattern (TCA Wing/Body/LE Flap Configuration M_∞= 0.95, α= 18.3°, Re_c= 40 million)

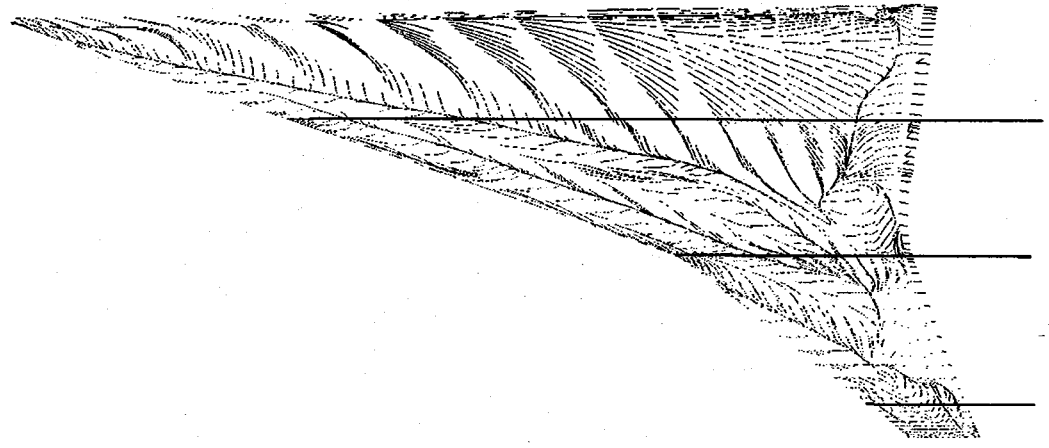

"True" Degani–Schiff

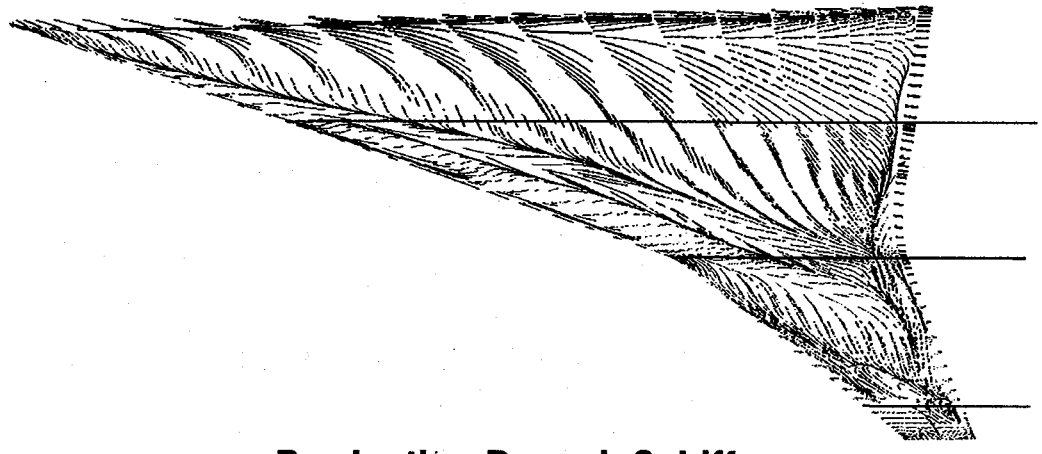

Production Degani–Schiff

Effect of "True" Degani-Schiff/Grid-Modification

The summary of the computed lift and drag for each computed configuration is given in the table below. The cumulative difference in lift force from applying all of the changes, the turbulence model, refined forebody region, and wing-vortex grids, is 2.4%. That these changes in lift are small is possibly due to the excessive amounts of dissipation that were required to compute the solutions using the given grid system. While the trends appear rational, the quantitative differences cannot be stated with any certainty.

At the three labeled spanwise stations in the chart below, the pressure distributions for both computations are compared. These stations correspond to y/b = 0.31, y/b = 0.61, and y/b = 0.93 all referenced to the body centerline. Examining the first inboard station, y/b = 0.31, the OVERFLOW implementation is predicting a primary vortex suction peak at x/c = 0.25, and a small induced secondary vortex suction peak at about x/c = 0.10. The original implementation of the Degani-Schiff modifications is predicting a weaker primary vortex suction peak located closer to x/c = 0.3, but also a strong distinct secondary suction peak at x/c = 0.10 and a small tertiary suction peak at x/c = 0.175. The OVERFLOW implementation predicts a shock near the trailing edge, while the original implementation is obviously having problems in this region. At the wing break, y/b = 0.6, the two implementations are showing similar behavior. The original Degani-Schiff implementation is better able to capture the distinct suction peaks from the different primary and secondary vortices which combine in this section. At the outboard section, y/b = 0.93, there are relatively large differences between the predicted pressure distributions for the two implementations. This is due to the presence of unsteadiness in the computations. All of the computations were run in a non-time-accurate mode in order to accelerate the convergence in the inviscid flow regions. This was done primarily due to time constraints within the study.

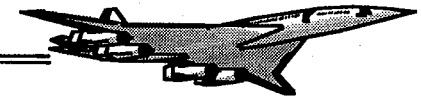

Effect of "True" Degani-Schiff/Grid-Modification

- 2.4% Increase in lift with change in turbulence model:

Case	C_L	C_{Lwing}	C_D	L/D
Production	0.823	0.717	0.25	3.28
True D-S	0.829	0.718	0.25	3.32
Fuselage Grid	0.835	0.717	0.25	3.36
Fuse + Vortex Grid	0.841	0.723	0.26	3.23

- Variation in pressures:

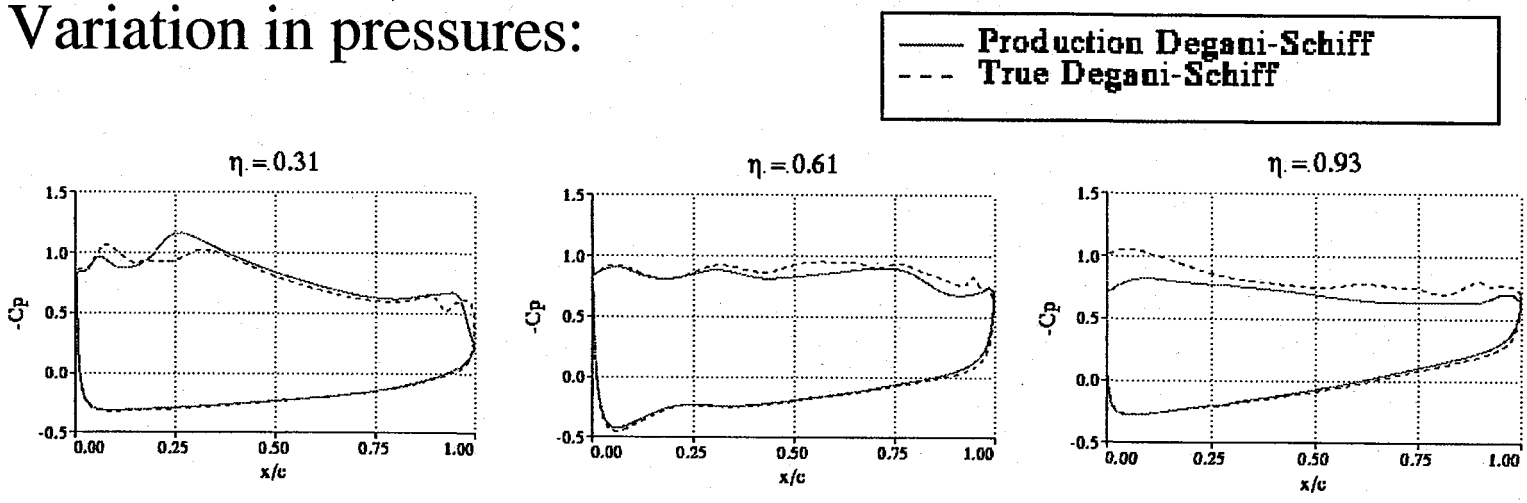

Summary/Conclusion

A process has been established for CFD data generation for the nonlinear loads database. The process was initially developed on the M2.4-7A configuration and applied subsequently to the TCA configuration

Convergence criteria for loads were established and quantities describing the variations of sectional properties were monitored.

The use of time-accurate simulations alleviated some of the numerical unsteadiness that caused large variations in sectional loads, especially at the outboard wing section.

However, the flowfield for higher angles-of-attack seems to be dominated by the wing primary vortex. Therefore, the uncertainties associated with the turbulence model and grid resolution could not be quantified with certainty since the variation in the integrated quantities were rather small (2.4%) compared to the strength of the wing primary vortex.

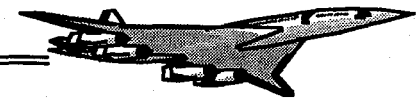

Summary/Conclusion

- Process established for CFD data generation for nonlinear loads database
- Loads convergence criteria were established
- Use of time-accurate simulations improved convergence
- Some uncertainty of turbulence model/grid - flowfield dominated by the wing apex primary vortex

Possible Further Studies

The use of larger time-steps will help a faster convergence of the solutions. However, the use of more sub-iterations would be necessary. The Reynolds number effects are to be investigated in order to establish confidence in the database obtained at 40 million. The same turbulence model comparison study that was performed for Mach 0.95 needs to be done for supersonic Mach numbers where boundary layers are thinner and vortices flatter. The use of smoother grids (in other words grids that have less spanwise stretching due to flap segments) is highly recommended. Finally, in the framework of assessing the effect of turbulence models modifications to the Spalart Allmarras turbulence model for vortical flows should be investigated.

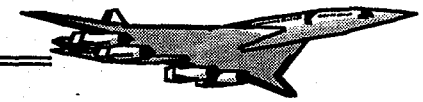

Possible Further Studies

- ❑ Use of larger time steps (with more sub-iterations?)
- ❑ Assess effects of Re number
- ❑ Turbulence model comparison study at supersonic Mach numbers
- ❑ Smoother grids (less stretching at flap segments)
- ❑ Modifications to the S-A model for vortical flows for further uncertainty assessments